COMMUNICATION

Integrated Freestanding Two-dimensional Transition Metal Dichalcogenides

*Hyun Jeong, Hye Min Oh, Anisha Gokarna, Hyun Kim, Seok Joon Yun, Gang Hee Han, Mun Seok Jeong, Young Hee Lee, and Gilles Lerondel**

This paper reports on the integration of freestanding transition metal dichalcogenides (TMDs). Monolayer (1-L) MoS_2, WS_2, and WSe_2 as representative TMDs are transferred on ZnO nanorods (NRs), used here as nanostructured substrates. The photoluminescence (PL) spectra of 1-L TMDs on NRs show a giant PL intensity enhancement, compared with those of 1-L TMDs on SiO_2. The strong increases in Raman and PL intensities, along with the characteristic peak shifts, confirm the absence of stress in the TMDs on NRs. In depth analysis of the PL emission also reveals that the ratio between the exciton and trion peak intensity is almost not modified after transfer. The latter shows that the effect of charge transfer between the 1-L TMDs and ZnO NRs is here negligible. Furthermore, confocal PL and Raman spectroscopy reveal a fairly consistent distribution of PL and Raman intensities. These observations are in agreement with a very limited points contact between the support and the 1-L TMDs. The entire process reported here is scalable and may pave the way for the development of very efficient ultrathin optoelectronics.

2D transition metal dichalcogenides (TMDs), which are atomically thin semiconductors consisting of transition metals M-(Mo, W, Sn, etc.) covalently bonded to chalcogens X-(S, Se, Te), have recently been the focus of extensive research activity.[1–4] In particular, group VI monolayer (1-L) TMDs with chemical formula MX_2 (M = Mo, W; X = S, Se) are promising materials for ultrathin photodetectors, light-emitting devices, and photovoltaic systems, owing to their direct band gap with relatively intense photoluminescence (PL).[5–7] However, the optical properties and crystalline quality of 1-L TMDs integrated on planar substrates are still not satisfactory for practical application because of the substantial strain. The crystalline strain, which is attributed to the lattice mismatch between the 1-L TMD and the inhomogeneous substrate,[8–10] can alter the electronic band structure of the 1-L TMD by modulating the lattice constant and van der Waals gap.[11–13] According to previous reports, the band gap energy of 1-L TMD changes from direct to indirect upon increase of the crystalline strain.[14–18] To overcome the negative effect of strain, several research groups have experimentally and theoretically investigated locally strain-free TMDs. Castellanos-Gomez et al.[19] discussed the mechanical properties of freely suspended MoS_2 nanosheets, while Shi et al.[20] investigated exciton dynamics in suspended 1-L and few-layer MoS_2. Notably, suspended TMDs have better crystalline and optical qualities than supported TMDs, resulting in improved device performances.[20–22] However, previously reported suspended TMDs suffer from a substantial limitation, i.e., strain-free regions are localized in small areas of the TMDs. For practical applications such as integrated optoelectronics, freestanding 1-L TMDs over a large surface area are required. Notably, integrated freestanding 1-L TMDs exhibiting enhanced optical properties over the whole area have not been systematically obtained yet.

Herein, we report the integration of freestanding 1-L TMDs on nanostructured substrates. As 1-L TMD materials, MoS_2, WS_2, and WSe_2 with optical band gaps of 1.84, 2.00, and 1.62 eV, respectively, were used.[23–25] These materials are representative luminescent 1-L TMDs having a direct band gap. They are widely studied for various applications such as transistors, photodetectors, and light-emitting devices. ZnO nanorods (NRs) grown by chemical bath deposition (CBD) on a silicon substrate were used as nanostructured substrates. In addition to being an easy and scalable process, the combination of 1-L TMDs with ZnO NRs is promising for integrated optoelectronics because ZnO is a direct band gap semiconductor with a wide band gap of 3.2 eV.[26] Scanning electron microscopy (SEM) was used to observe the morphology of the 1-L TMDs on the ZnO NRs. The optical properties were examined by room

Dr. H. Jeong, Dr. A. Gokarna, Prof. G. Lerondel
Laboratoire de Nanotechnologie et d'Instrumentation Optique
Institut Charles Delaunay
CNRS-UMR 6281
Université de Technologie de Troyes
BP 2060, 10010 Troyes, France
E-mail: gilles.lerondel@utt.fr
Dr. H. M. Oh, H. Kim, S. J. Yun,
Dr. G. H. Han, Prof. M. S. Jeong, Prof. Y. H. Lee
Center for Integrated Nanostructure Physics
Institute for Basic Science
Sungkyunkwan University
Suwon 440-746, Republic of Korea
Dr. H. M. Oh, H. Kim, S. J. Yun,
Prof. M. S. Jeong, Prof. Y. H. Lee, Prof. G. Lerondel
Department of Energy Science
Sungkyunkwan University
Suwon 440-746, Republic of Korea

DOI: 10.1002/adma.201700308

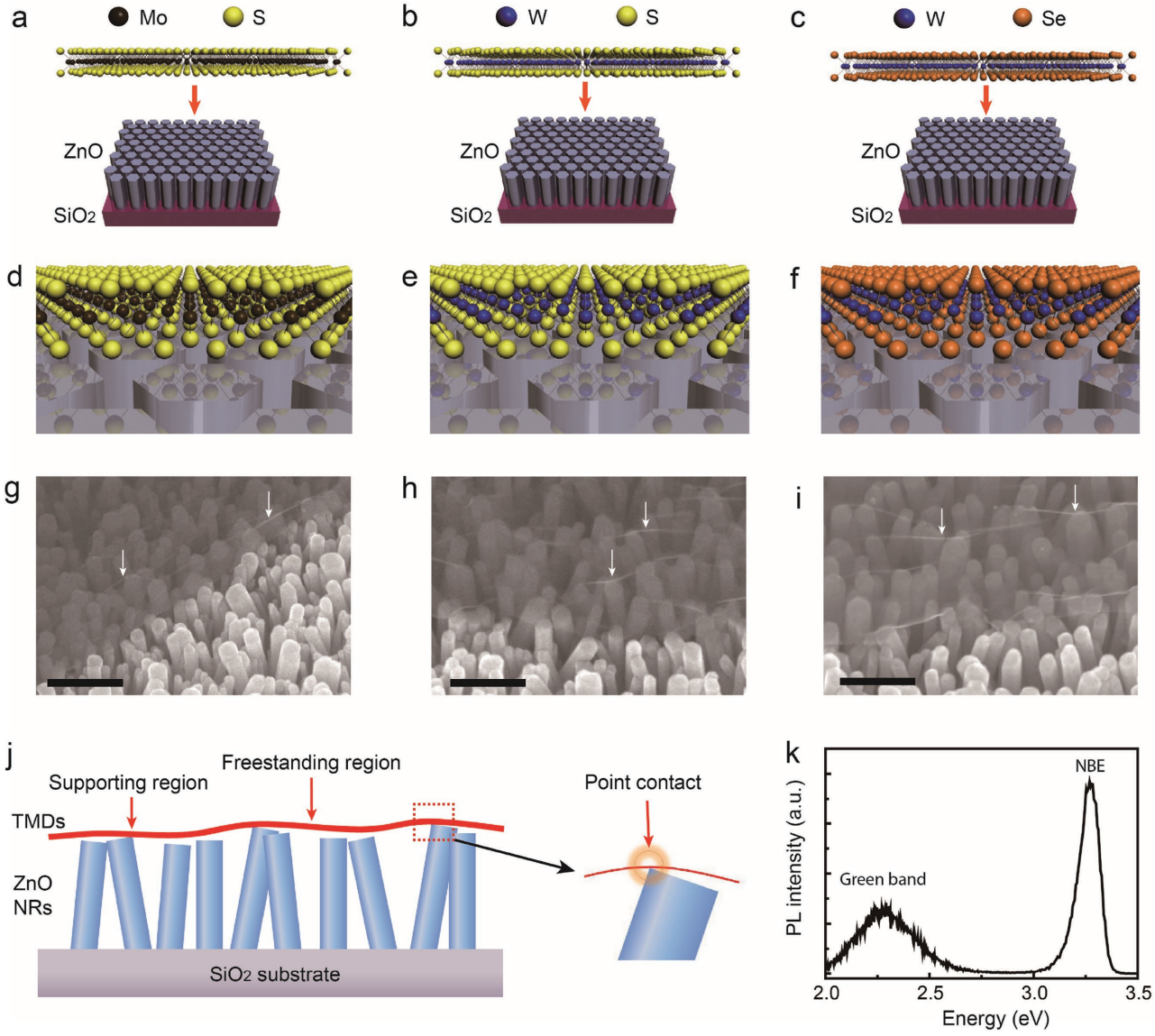

Figure 1. Fabrication and concept of integration of freestanding 1-L TMDs on NRs. 3D schematics of the simplified fabrication process of 1-L a) MoS_2, b) WS_2, and c) WSe_2 on ZnO NRs. The TMDs were transferred onto the NRs by a wet-transfer method. Magnified 3D schematics of 1-L d) MoS_2, e) WS_2, and f) WSe_2 on the NRs. Scanning electron microscopy images of the edge of 1-L g) MoS_2, h) WS_2, and i) WSe_2 on the ZnO NRs. The 1-L TMDs were partially supported by the NRs. j) Cross-sectional schematic of 1-L TMDs supported by the NRs. The contact between the 1-L TMDs and the NRs supposedly occurs only at the edge of the ZnO NRs. k) Room temperature PL spectrum of the ZnO NRs.

temperature PL and Raman spectroscopy. Besides, confocal scanning PL and Raman spectroscopy were employed to assess the spatially resolved optical properties.

In this work, l-L MoS_2, WS_2, and WSe_2 were grown by chemical vapor deposition (CVD) on SiO_2/Si substrates. ZnO NRs (average diameter of ≈50 nm) were synthesized by the CBD method on the SiO_2 substrate (Figure S1, Supporting Information). To form integrated freestanding TMDs, the 1-L TMDs grown by CVD were transferred onto the NRs. The transfer process was conducted as follows: polymethylmethacrylate (PMMA) was coated on the as-grown 1-L TMDs to support them during the chemical etching of SiO_2 by a diluted HF solution. Upon separation from the SiO_2 substrate, the 1-L TMDs with PMMA were transferred to a prepared template consisting of ZnO NRs on an Si substrate. To remove the residual water, the 1-L TMDs were dried at 80 °C for 1 h. The simplified fabrication processes used to form the integrated freestanding MoS_2, WS_2, and WSe_2 on NRs are illustrated in **Figure 1**a–c. The Mo, S, W, and Se atoms are represented by small spheres with dark brown, yellow, blue, and orange color, respectively. The transfer of each TMD onto the NRs and all the fabrication processes were conducted under ambient atmosphere at room temperature. The magnified 3D schematics for the suspended MoS_2, WS_2, and WSe_2 on ZnO NRs are depicted in Figure 1d–f, respectively. As the length of the ZnO NRs was not perfectly homogeneous, the transferred TMDs were,

presumably, partially supported by the NRs with a limited number of point contacts. The SEM images of the TMDs on the NRs are shown in Figure 1g–i. The black lines marked in each SEM image indicate a scale bar of 200 nm. The relatively dark areas in the SEM images in Figure 1g–i correspond to the 1-L MoS_2, WS_2, and WSe_2 regions on NRs, respectively. The weak wrinkles indicated by white arrows reveal that the TMDs are partially supported by the NRs. A cross-sectional schematic of the partially supported TMDs is shown in the SEM image in Figure 1j. The red line and blue pillars indicate the suspended TMDs and ZnO NRs, respectively. As marked by the red arrows, depending on the contact between TMDs and NRs, freestanding and supported regions can be found. In addition, owing to the high in-plane stiffness of the TMDs[27] and small diameter of the NRs (≈50 nm), only the edge of several NRs could be in actual contact with the TMDs. A few short wrinkles observable in the TMDs deposited on the NRs as shown by the SEM image support the idea of a very limited contact between the TMD monolayer and NRs. From the morphology of the TMDs on the NRs, we could assume that the TMDs are almost strain-free over the whole area. Figure 1k shows the room temperature PL spectrum of the investigated NRs used as supporting substrate. The PL spectrum exhibited a strong peak at 380 nm with a narrow bandwidth, which was caused by the exciton near-band-edge (NBE) transitions, and a weak peak at 500 nm with a broad bandwidth, which was related to the crystal defects.[28] The strong NBE peak with a weak green emission band confirmed that the ZnO NRs had high crystallinity and good optical properties.

To verify the optical properties of the suspended TMDs, we conducted PL measurements at room temperature. Notably, the PL peak intensities and positions provide information on the strain within the TMDs. The position of the PL signal is closely related to the band gap nature, namely, it reveals a direct or indirect transition.[29] For PL spectroscopy, a solid state laser (532 nm) was used as an excitation source along with a 30 cm monochromator equipped with a 150 groove/500 nm blazed grating. The PL spectra of the 1-L MoS_2, WS_2, and WSe_2 on the ZnO NRs are shown in **Figure 2**a–c, respectively, together with the PL spectra of the same TMDs deposited on the SiO_2 substrates. The PL spectra of the TMDs on NRs and SiO_2 substrates are represented in red and black colors, respectively. In Figure 2a, the PL peaks for the A and B excitons, which are attributed to direct optical transitions, are marked. The difference of peak energy between the A and B excitons is usually ascribed to the spin-orbital splitting of the valence band.[5] As the PL peak intensities of the TMDs on the NRs were significantly larger than those of the TMDs on SiO_2 substrate, the PL of the latter was multiplied by a factor of 10, as marked in each PL spectrum. As shown in Figure 2a, although the peaks of the A and B excitons were observed in both the 1-L MoS_2 on the NRs and the SiO_2 substrate, the intensity of the B exciton peak of 1-L MoS_2 on NRs was significantly lower than that of 1-L MoS_2 on SiO_2. However, the integrated PL intensity of 1-L MoS_2 on the NRs, including both the A and B exciton peaks, was more than 150 times higher than that of 1-L MoS_2 on the SiO_2 substrate. A similar tendency was observed in the PL spectra of 1-L WS_2 and WSe_2. The PL intensities of the partially supported 1-L WS_2 and WSe_2 were 50 and 158 times higher than those of 1-L WS_2 and WSe_2 on SiO_2, respectively. The PL intensities of TMDs can be affected by several factors such as crystalline quality, doping, and strain. In this study, the influence of the crystalline quality can be excluded because we deposited identical CVD-grown TMDs on both ZnO NRs and SiO_2 substrates. Possible doping effect of 1-L TMDs by contacting with ZnO cannot be excluded in our case because the work function of ZnO is higher than the electron affinity of all the 1-L TMDs (Figure S2, Supporting Information). Therefore, photoexcited electrons of 1-L TMDs could be transferred to ZnO at the contact point. However, according to previous reports, PL intensities of 1-L MoS_2 and 1-L WS_2 are not more than three times increased by charge transfer.[30,31] Moreover, PL intensity of 1-L WSe_2 is decreased by photoexcited electron transfer.[32] It means that charge transfer occurring in 1-L TMDs on ZnO NRs has minor effect in this study as a strongly enhanced PL intensity is observed as presented in Figure 2a–c. Consequently, we believe that the enhancement in PL intensity is due to the decrease of strain in the 1-L TMD. According to previous reports in terms of strain, the integrated PL intensities of 1-L MoS_2, WS_2, and WSe_2 were enhanced by 2, 1.5, and 20 times, respectively, when the strain was reduced by 2%.[16,33,34] From these earlier reports and considering the enhancement factor observed in our case (up to two orders of magnitude), we can presume that the TMDs on the NRs are almost strain free. Our observations are in agreement with recently published theoretical predictions on 2D phosphorene.[35] Analog results have also been obtained in the case of III-V semiconductor quantum wells, leading to indirect-to-direct band gap engineering.[36]

The normalized PL spectra of 1-L MoS_2, WS_2, and WSe_2 on the NRs and SiO_2 are shown in Figure 2d–f, respectively. This representation allows conducting a detailed comparison between the peak positions and shapes of the PL spectra. As shown in Figure 2d, the peak energies of the A exciton in 1-L MoS_2 on the NRs and SiO_2 were 1.89 and 1.84 eV, respectively. The full width at half maximum (FWHM) of the A exciton peak for 1-L MoS_2 on the NRs was 80 meV, while that for 1-L MoS_2 on SiO_2 was 126 meV. The peak energies of the A exciton for 1-L WS_2 on the NRs and SiO_2 were 2.03 and 2.00 eV, respectively. The FWHM of the A exciton for 1-L WS_2 on the NRs was 51 meV, whereas the FWHM for 1-L WS_2 on SiO_2 was 85 meV. The blue shift in the peak position and the considerable decrease in FWHM, shown in the PL spectra, are in accordance with previously reported PL results of strain-relaxed 1-L MoS_2 and WS_2.[16,33] The enormous increase in PL intensity of the A exciton, compared with the B exciton, shown in the PL spectra of 1-L MoS_2 and WS_2 on the NRs, is attributed to the increased number of A excitons induced by strain relaxation. As for the 1-L WSe_2 TMD, the peak energies of the A exciton for the layers deposited on the NRs and SiO_2 substrate were 1.66 and 1.62 eV, respectively. The FWHM for the layer deposited on the NRs was 70 meV, whereas that for the layer on SiO_2 was 85 meV. Similar to the two other 1-L TMDs, the blue shift of the peak position and increase in FWHM, observed in the PL spectrum of 1-L WSe_2 on the NRs, are in agreement with the PL results previously obtained on strain-relaxed WSe_2.[34] The blue-shifted PL peaks and increased PL intensities of 1-L TMDs on the NRs correspond to suspended 1-L TMD as previously reported.[37]

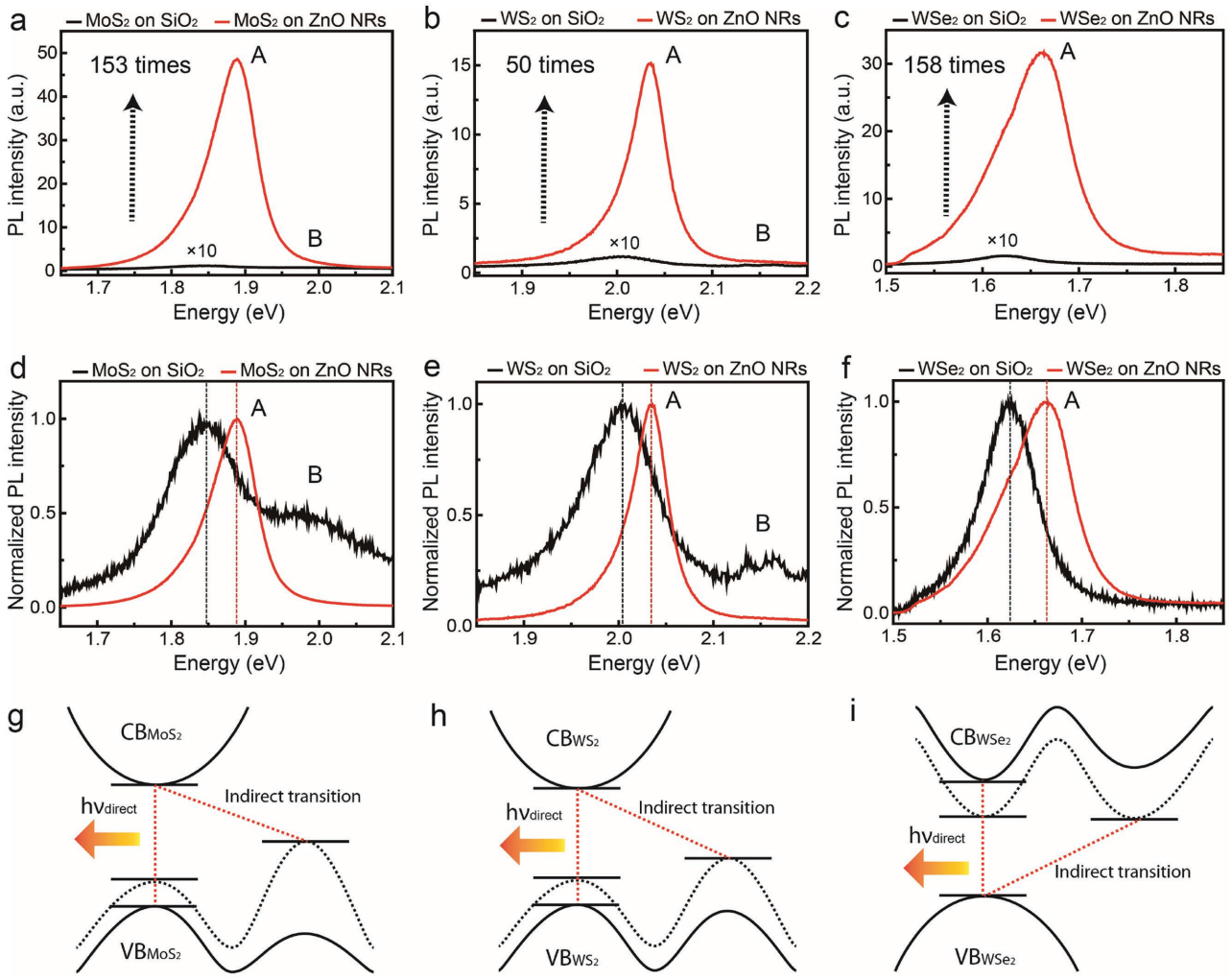

Figure 2. Enhanced PL properties of 1-L TMDs on NRs. PL spectra of 1-L a) MoS_2, b) WS_2, and c) WSe_2 on the ZnO NRs and on SiO_2 substrates as references. Enhanced PL intensities were observed for 1-L TMDs on the NRs, compared with the reference samples. Normalized PL spectra for 1-L d) MoS_2, e) WS_2, and f) WSe_2 on the NRs and on SiO_2. The position and full width at half maximum of the peaks of the 1-L TMDs on the NRs are considerably different from those of the 1-L TMDs on SiO_2. Energy band diagrams of 1-L g) MoS_2, h) WS_2, and i) WSe_2 on ZnO NRs compared with those obtained for the same TMDs deposited on SiO_2.

To interpret the origin of the PL enhancement and peak shift, energy band diagrams showing optical transitions of 1-L TMDs on the NRs and SiO_2 are depicted in Figure 2g–i. As the TMD optical transitions are closely correlated with the lattice constant, which is itself strain dependent, a possible optical transition based on PL results and previous research can be expected.[16,33,34] The solid and dotted lines indicate 1-L TMDs on NRs and SiO_2, respectively. The valence band maximum for 1-L MoS_2 and WS_2 on the NRs matches with the minimum of the conduction band, resulting in enhanced PL intensity with increased band gap when the strain is relaxed, as illustrated in Figure 2g,h.[16,33] On the other hand, the enhanced PL intensity of 1-L WSe_2 on the NRs could be due to a shift of the minimum of the conduction band, which would then match the maximum of the valence band, as depicted in Figure 2i.[34] From the PL analysis of TMDs on the ZnO NRs, we infer that 1-L TMDs on NRs behave almost as freestanding crystals.

To confirm the absence of influence of the charge transfer in the PL enhancement, we analyzed the exciton peaks embedded in the PL spectra of the integrated monolayers. Lorentzian fitting and intensity normalization were applied for all the PL spectra to compare the peaks position and intensity. Top and bottom of **Figure 3**a show normalized PL spectra with fitted exciton and trion peaks of 1-L MoS_2 on ZnO NRs and SiO_2, respectively. For all the PL spectra, black squares indicate raw data points and red solid line is for fitted PL spectra. Embedded peaks for negative trion (X^-), A exciton (X), and B exciton are represented as blue, red, and green curves, respectively. The B exciton peak is very weak in the PL spectrum of 1-L MoS_2 on ZnO NRs confirming that the PL enhancement is attributed to the reduced strain in the film. Both X^- and X peaks of the 1-L MoS_2 on ZnO NRs PL are shifted to higher energy as to compare the 1-L MoS_2 on SiO_2. Here again this shift can be attributed to the absence of strain in the films.[33] The intensity ratio of the trion and exciton (I_x^-/I_x) peaks shown

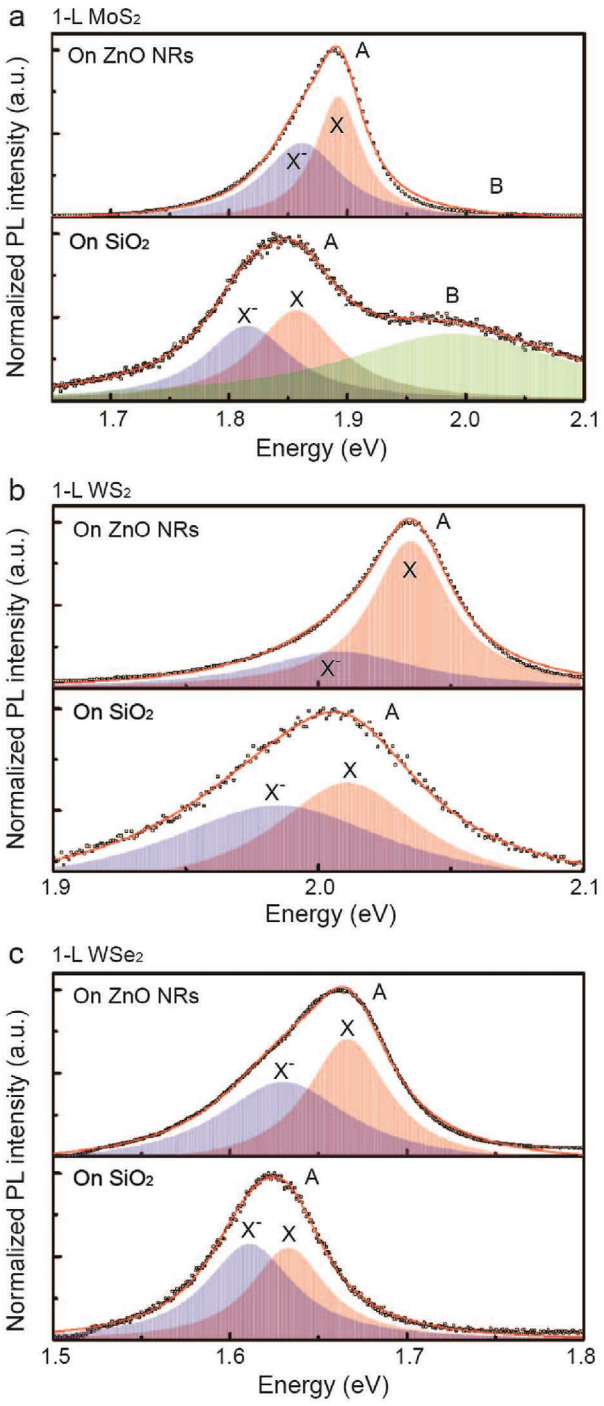

Figure 3. Excitonic analysis of the PL emission. Fitted PL spectra of the 1-L a) MoS_2, b) WS_2, and c) WSe_2 on the ZnO NRs (top) and on SiO_2 (down) substrates. A clear shift of the A exciton (X and X^-) is observed whatever the material as expected from strain relaxation. The disappearing of the B exciton peak in the case of MoS_2 is also consistent with strain relaxation. As for the possible charge transfer, two observations indicate that this process is not significant here, the presence of the X^- in all spectra and secondly the ratio between the X and X^- remains almost unchanged except for WS_2 where a slight decrease of X^- peak is observed. This is consistent with the band energy diagram as discussed in the Supporting Information. All these observations confirm the new proposed concept of very limited point contact between the support and the 1-L TMDs.

in 1-L MoS_2 on ZnO NRs PL is slightly lower than that of the 1-L MoS_2 on SiO_2. As for the presence of the negative trion in the PL spectrum of 1-L MoS_2 on ZnO NRs implies that several photoexcited electrons of the 1-L MoS_2 were transferred to the ZnO NRs. The fitted PL spectra of the 1-L WS_2 transferred on ZnO NRs and on SiO_2 are shown at the top and bottom of Figure 3b. The peaks for the X^- and X in the case of the 1-L WS_2 on ZnO NRs are also shifted to higher energy compared with the ones of the 1-L WS_2 on SiO_2. This effect is again due to reduced strain.[16] The intensity of the trion peak revealed in the PL spectrum of the 1-L WS_2 on the ZnO NRs is lower than that of the 1-L WS_2 on SiO_2. Finally, Figure 3c shows the fitted PL spectra of the 1-L WSe_2 on ZnO NRs (top) and SiO_2 (bottom) with embedded trion and exciton peaks. Both X^- and X peaks of 1-L WSe_2 on ZnO NRs display a blue shift compared with those of the 1-L WSe_2 on SiO_2. Intensity of X^- peak observed from the 1-L WSe_2 on ZnO NRs is slightly decreased as to compared with the peak of the 1-L WSe_2 on SiO_2. A relatively higher increase of the X peak intensity presented in PL spectrum of the 1-L WS_2 as to compared with the 1-L MoS_2 and 1-L WSe_2 is attributed to charge transfer which correspondingly lies in a smaller PL enhancement as observed in the 1-L WS_2. This can be interpreted by so limited a larger contact area of the 1-L WS_2 as to compared with the one of 1-L MoS_2 and 1-L WSe_2 deposited on ZnO NRs. This is due to different in-plane stiffness.[38] However, enhancement of the PL intensity observed in 1-L WS_2 is still tremendous even though charge transfer may have occurred. From Figure 3, we found that the PL enhancement of the 1-L TMDs on ZnO NRs observed here is mostly due to the strain relaxation. In addition, local PL spectra taken on freestanding and supporting regions of 1-L TMDs on ZnO NRs substantiate that PL intensities of 1-L TMDs on ZnO NRs are not significantly affected by charge transfer (Figure S3, Supporting Information). This confirms that strain relaxation of the 1-L TMDs is the predominant effect for enhancement of the PL intensity observed in 1-L TMDs on ZnO NRs.

To verify that the strain of the 1-L TMDs deposited on the NRs are relaxed, we investigated the phonon modes of each 1-L TMD by using confocal Raman spectroscopy, as the 1-L TMD lattice vibration is significantly sensitive to strain. A solid-state laser (532 nm) was used as an excitation source, while an 1800 groove/500 nm blazed grating was used for the Raman spectroscopy. The 3D schematics for the vibration modes of 1-L MoS_2, WS_2, and WSe_2 are depicted in **Figure 4**a–c, respectively. As the E^1_{2g} mode involves the in-plane vibration and the A_{1g} mode corresponds to the out-of-plane vibration, the E^1_{2g} mode is typically more sensitive to strain than the A_{1g} mode in 1-L TMDs.[39] The Raman spectra of the 1-L TMDs are shown in Figure 4d–f. The red spectra belong to 1-L TMDs on the NRs, while the black spectra belong to 1-L TMDs on SiO_2. The E^1_{2g} and A_{1g} modes for 1-L MoS_2, WS_2, WSe_2 were clearly observed in the Raman spectra, as marked in Figure 4d–f. However, the Raman mode intensities of the TMDs on the NRs were enormously higher than those of the TMDs on SiO_2. To observe the shape and peak position of each Raman mode, all the Raman spectra were normalized, as shown in Figure 4g–i. The A_{1g} modes for 1-L MoS_2 on both the NRs and SiO_2 were observed at 403.5 cm^{-1}. The E^1_{2g} mode of 1-L MoS_2 on the NRs was observed at 384.5 cm^{-1}, while that of 1-L MoS_2 on SiO_2 was

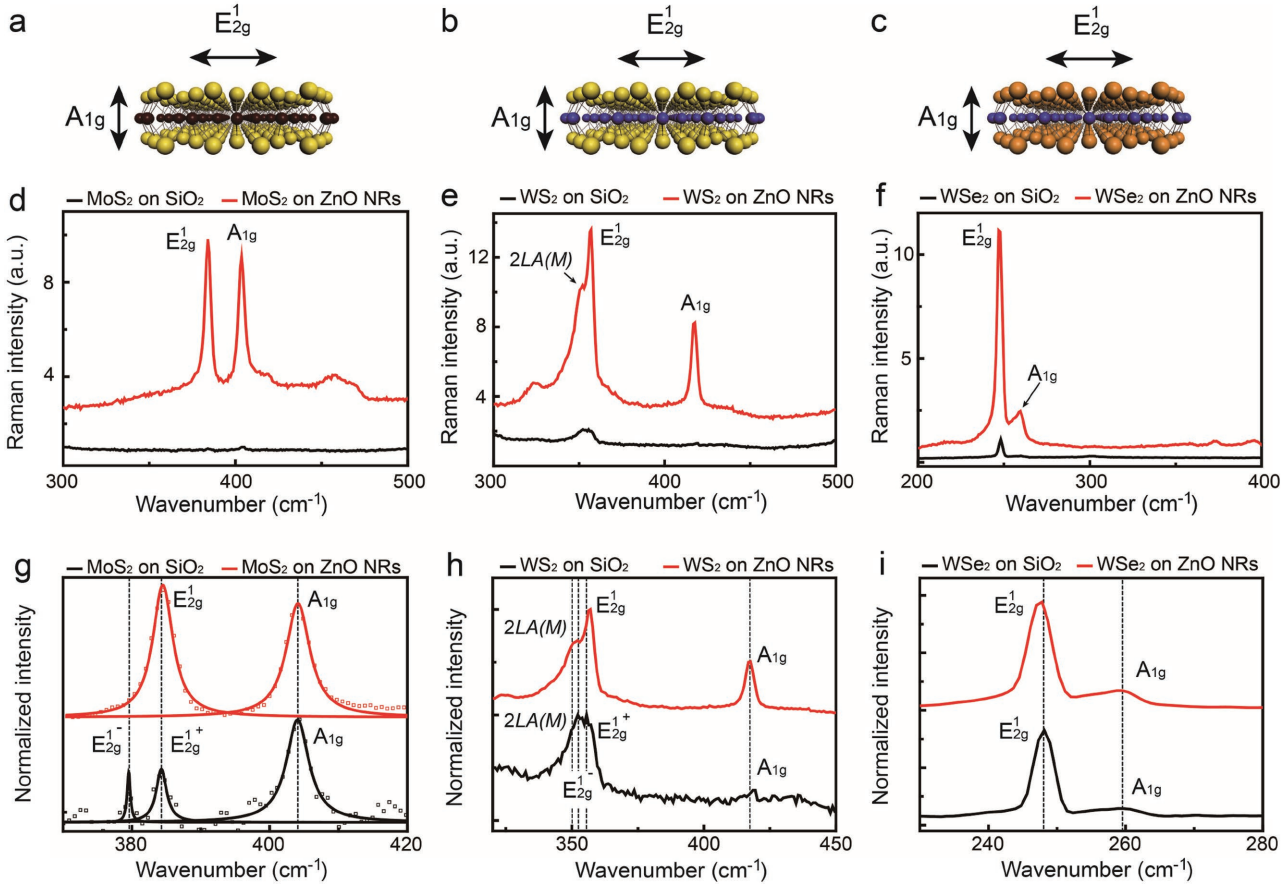

Figure 4. Raman scattering of 1-L TMDs on NRs for crystalline strain analysis. 3D schematics of 1-L a) MoS_2, b) WS_2, and c) WSe_2 illustrated with representative Raman modes. Raman spectra of 1-L d) MoS_2, e) WS_2, and f) WSe_2 on ZnO NRs and on SiO_2 substrate (as references). Outstanding increases in Raman intensities were observed in 1-L TMDs on the ZnO NRs, compared with the references. Intensity normalized Raman spectra of 1-L g) MoS_2, h) WS_2, and i) WSe_2 on the NRs with references. Characteristic shifts in the Raman modes and intensity variations were observed in 1-L TMDs on the NRs, compared with the reference samples.

split in $E^1_{2g}{}^+$ (384.2 cm^{-1}) and $E^1_{2g}{}^-$ (379.5 cm^{-1}), as shown in Figure 4g. The increased Raman intensity and nonsplitting of the E^1_{2g} Raman mode are in accordance with a strain-relaxed and suspended 1-L MoS_2 TMD.[33,40] The 2LA(M), E^1_{2g}, and A_{1g} mode of 1-L WS_2 on the NRs were observed at 352.0, 356.6, and 417.2 cm^{-1}, respectively, as presented in Figure 4h.[41] In the 1-L WS_2 on SiO_2, the E^1_{2g} mode was split into $E^1_{2g}{}^+$ (355.5 cm^{-1}) and $E^1_{2g}{}^-$ (352.2 cm^{-1}). Furthermore, the intensity of the A_{1g} mode was significantly reduced in the 1-L WS_2 on SiO_2. The nonsplitting and modest blue shift observed in the E^1_{2g} mode, along with the reduced intensity of the A_{1g} mode, indicated that the strain of 1-L WS_2 on the NRs was lower than that of 1-L WS_2 on SiO_2.[16] The E^1_{2g} modes for 1-L WSe_2 on the NRs and SiO_2 were at 247.2 and 248.2 cm^{-1}, respectively, as shown in Figure 4i. The peak positions of the A_{1g} mode (259.1 cm^{-1}) for 1-L WSe_2 on the NRs and SiO_2 were almost identical. However, the peak intensity of 1-L WSe_2 on the NRs was stronger than that of 1-L WSe_2 on SiO_2. The enhanced intensity and the red-shifted E^1_{2g} mode, together with the increased intensity of the A_{1g} mode, revealed the presence of relaxed 1-L WSe_2.[34] The Raman measurements confirmed that the TMDs deposited on the ZnO NRs had significantly lower strain than those deposited on SiO_2, confirming that the huge enhancement in the PL intensities of TMDs on the NRs is closely related to the relaxation of the crystalline strain and changes in the nature of the band gap energy.

To directly observe the integration of freestanding TMDs on NRs, spatially resolved optical characterization was conducted by using confocal PL and Raman spectroscopy. A piezoelectric scanner, a high numerical aperture (0.7) objective lens, and a pinhole (10 μm) were employed to obtain confocal PL and Raman images. The SEM images of 1-L MoS_2, WS_2, and WSe_2 on the NRs are shown in Figure 5a–c, respectively. The length of the scale bar in all the SEM images is 5 μm. A single 1-L MoS_2 flake with a triangular shape and no visible cracks can be clearly observed in the SEM image (**Figure 5**a); on the other hand, cracked flakes were found in 1-L WS_2 and WSe_2, as shown in Figure 5b,c, respectively. Possibly, the flakes were divided because of incomplete in-plane coalescence, which is typical of CVD-grown 1-L TMDs. However, each flake still exhibited a small area of micrometer dimensions. In addition, the relatively smaller PL intensity enhancement of 1-L WS_2 on the NRs, compared with that of 1-L MoS_2 and WS_2 on the NRs, was attributed to large separation between the flakes.

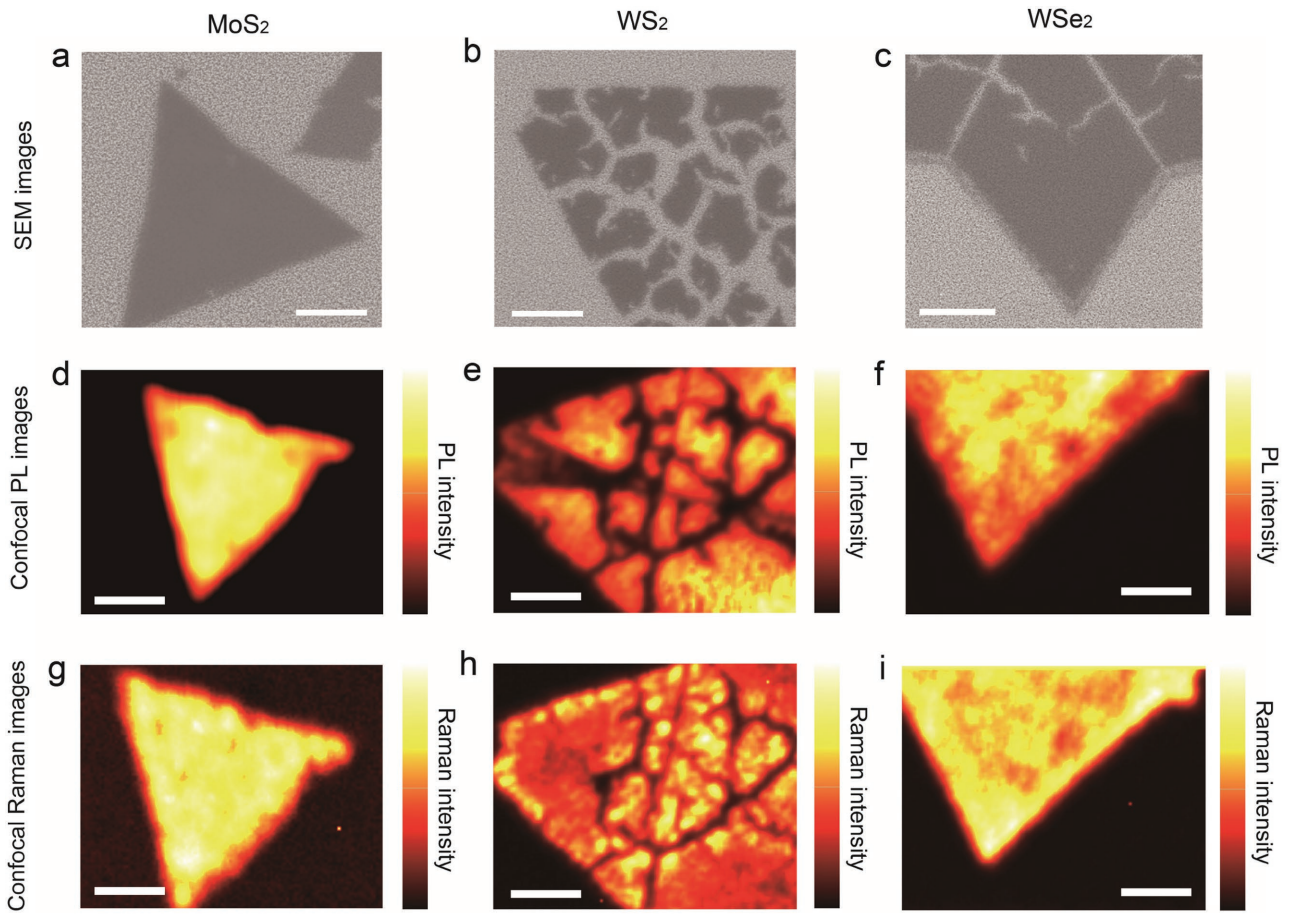

Figure 5. Confocal PL and Raman images of integrated freestanding TMDs on NRs. Scanning electron microscopy images of 1-L a) MoS_2, b) WS_2, and c) WSe_2 on ZnO NRs. The separated flakes in 1-L WS_2 and WSe_2 are possibly due to incomplete in-plane coalescence. Confocal PL images of 1-L d) MoS_2, e) WS_2, and f) WSe_2 on the ZnO NRs. The PL intensities of 1-L TMDs on ZnO NRs are considerably consistent within a single flake. Confocal Raman images of 1-L g) MoS_2, h) WS_2, and i) WSe_2 on the NRs. Fairly homogeneous Raman intensities are observed for 1-L TMDs on the NRs.

The confocal PL images of 1-L MoS_2, WS_2, and WSe_2 on NRs are shown in Figure 5d–f, respectively. The length of the scale bar for all the confocal PL and Raman images is 2 µm. The PL intensity of 1-L MoS_2 on NRs was revealed to be considerably consistent over the whole area of the flake, as shown in Figure 5d. For 1-L WS_2, the PL intensity remained noticeably unchanged within a single flake area, although the flakes were separated (Figure 5e). As shown in Figure 5f, the PL intensity on the 1-L WSe_2 flake was fairly homogeneous, even though less uniform than that of 1-L MoS_2. The relatively weaker PL intensity at the edge of the flake is a typical feature of CVD-grown 1-L WSe_2. The confocal PL images of TMDs on the NRs show enhanced PL intensities over the whole area of the TMD flakes supported by the ZnO NRs. The confocal Raman images for 1-L MoS_2, WS_2, and WSe_2 on the NRs are shown in Figure 5g–i, respectively. The Raman intensity of 1-L MoS_2 was found to be remarkably constant over the whole area of the flake (Figure 5g). In the confocal Raman image of 1-L WS_2 (Figure 5h), the Raman intensity is still noticeably homogeneous in each individual flake. However, the fluctuation of the Raman intensity is higher than that of the PL intensity. This is attributed to a local contact area between 1-L WS_2 and the ZnO NRs. Indeed, the Raman signal is more sensitive to strain than the PL signal. Appreciably uniform Raman intensity was observed in 1-L WSe_2 on the NRs, as shown in Figure 5i. The peak position and width of the E^1_{2g} Raman mode for TMDs on the NRs were found to be considerably uniform over the whole area of a single flake (Figures S4–S6, Supporting Information). The confocal Raman images of TMDs on NRs provided significantly clear evidence that the TMDs integrated on the NRs were freestanding crystals.

To confirm the extremely limited contact area between the 1-L TMDs and the NRs, morphological analysis has been performed using high-resolution SEM images with different magnifications. **Figure 6**a–c shows plane-view SEM images of 1-L MoS_2 on NRs. The scale bars revealed in Figure 6a–c indicate 5, 1, and 0.2 µm, respectively. As shown in low magnification SEM image (Figure 6a), the relatively dark region is the 1-L MoS_2. The small bright and widely distributed dots are the ZnO NRs. The small bright dots are ZnO NRs. The surface of 1-L MoS_2 seems perfectly uniform in the low magnification SEM image. Moreover, the 1-L MoS_2 presents still homogeneous morphology without any wrinkles in the middle magnification SEM image (Figure 6b). The possibility to clearly observed the NRs

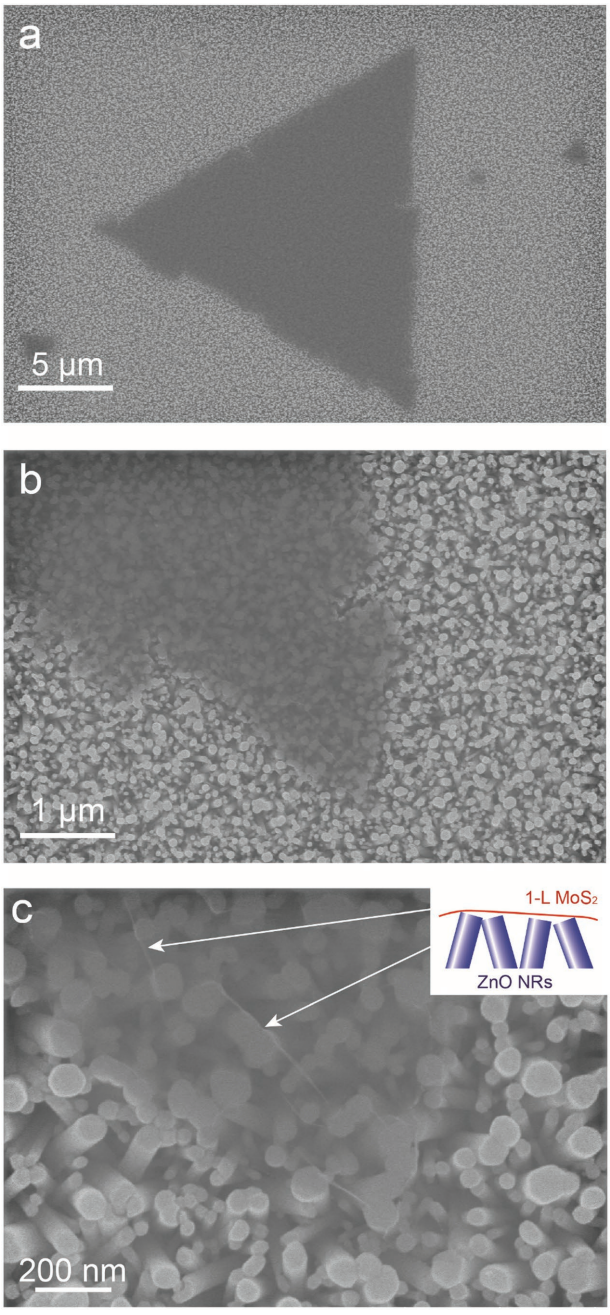

Figure 6. SEM of the transferred 1-L MoS_2 and NRs. SEM image of triangular 1-L MoS2 flake on NRs with a) low magnifications. Constant contrast shown in the low magnification SEM image reflects the homogeneity of the integrated suspended 1-L MoS_2. b) Middle magnification allows the NRs to be clearly resolved below and on the side of the monolayer. The uniformity of the contrast strongly suggests that the film is floating on the NRs. The freestanding nature of the monolayer is definitively confirmed by c) the high magnification image where very few wrinkles can be observed. At these points and only at these points, the 1-L MoS_2 and the NR are in contact. As sketched in the inset, this very limited contact area is due to the size, shape, and slight tilt of the NRs.

underneath the 1-L MoS_2, supports that the spatial resolution of the image is high enough to observe the few nanometers object but most importantly to reveal (if any) contrast change due to intimate contact between the TMDs monolayer and the NWs. Indeed, in the high magnification SEM image (Figure 6c), two lines of a few nanometer of width are observed as indicated by white arrows. These lines as shown in the inset are formed due to a point contact between the 1-L MoS_2 and the edge of the top of a NR. Further high magnification SEM image analysis reveals that the point contact only occurs at the edge of a very few number of specific NRs which are slightly longer. Based on the SEM image analysis, it is clear that the physical contact between the reported 1-L TMDs and the NRs is very limited. These observations support PL and Raman analysis that the tremendous emission enhancement is not related to the contact area but to direct optical transition allowed by the strain relaxation. This in turn, allows us to introduce the concept of integrated freestanding 1-L TMDs.

In conclusion, we have shown that the integration of two-dimensional freestanding TMDs is possible. Integration was performed using cheap and scalable substrates, i.e., ZnO NRs grown by CBD. As representative TMDs, 1-L MoS_2, WS_2, and WSe_2 were employed in this study. The integrated PL intensities of 1-L MoS_2, WS_2, and WSe_2 were found to be respectively 153, 50, and 158 times higher than the same 1-L TMDs transferred on SiO_2 substrates. Moreover, the blue shift in the position of the A exciton peak, observed for all the TMDs deposited on the NRs, confirmed that the enhancement in PL intensity was induced by strain relaxation. The analysis of exciton peaks embedded in PL spectra of 1-L TMDs on ZnO NRs supports that enhanced PL intensity is not considerably influenced by charge transfer phenomena. The enormous increases in Raman intensity and distinctive variations of the peak positions, observed in the Raman spectra of TMDs on the NRs, indicated that the strain was relaxed, compared with that of TMDs transferred on SiO_2. Fairly consistent distributions of PL and Raman intensities were observed in all the TMDs on the NRs, which were further confirmed by confocal PL and Raman spectroscopy. All the experimental results confirmed that the TMDs on the ZnO NRs were freestanding crystals. The same approach can also be extended to graphene and other TMD materials, and therefore also used to investigate the thermal properties. We firmly believe that our findings can lead to the development of a very promising high-performance technology, namely, strain-free-based two-dimensional TMD devices, and will also be helpful to extend the application of TMDs to large scale devices such as integrated circuits.

Experimental Section

Fabrication of Monolayer MoS_2: Monolayer (1-L) MoS_2 was grown by CVD. SiO_2 was used as the substrate. For the transfer of 1-L MoS_2, PMMA was coated onto as-grown 1-L MoS_2 as a support. Then, SiO_2 was etched in a dilute HF solution. The floating 1-L MoS_2 and PMMA were transferred onto the ZnO NRs and SiO_2 substrate. An acetone solution was used to remove PMMA. Finally, to eliminate the residual PMMA, the sample was dried at 80 °C for 1 h.

Fabrication of 1-L WX_2 (X = S, Se): 1-L tungsten dichalcogenides (WX_2; X = S, Se) were synthesized on SiO_2 substrates by the CVD method in atmospheric pressure. Ammonium metatungstate as a tungsten precursor was introduced with pure sulfur and selenium for the growth of WS_2 and WSe_2, respectively. Then, as-grown 1 L WX_2 was transferred onto the ZnO NRs by a conventional PMMA-supported wet-etching method. To minimize damages during the removal of PMMA

by the organic solvent, PMMA was annealed at 250 °C at low pressure (10^{-4} Torr) for 12 h.

Synthesis of ZnO Nanorods: The growth of ZnO NRs on the silicon substrate was conducted by adopting a chemical bath deposition technique. First, 0.025 M zinc acetate was dissolved in 250 mL of water; then, 0.3 mL of ammonium hydroxide was added to the solution and stirred at room temperature. The synthesis was conducted in the absence of metal catalysts or additives. The mixture was heated at 87 °C in a three-neck rounded bottom flask. The sample consisting of a ZnO seed layer previously deposited on silicon was immersed in the solution for 30 min. Thereafter, the sample was washed with water and dried in air.

Characterization: PL spectroscopy was performed by using a high numerical aperture (0.7) objective lens. Diode-pumped solid-state lasers (532 nm) were used as excitation sources for both the PL and Raman measurements. The Raman spectra were obtained in a typical backscattering geometry. Confocal PL and Raman mappings were obtained by multifunctional microscopy (NTEGRA, NT-MDT) with a pinhole. A 30 cm monochromator (SP2300, Princeton Instruments) was used to disperse the collected light from the samples. A thermoelectrically cooled charge-coupled device was used (PIXIS100, Princeton Instruments) for the detection of the optical signal.

Supporting Information

Supporting Information is available from the Wiley Online Library or from the author.

Acknowledgements

This work was supported by the FUI MULTISS project (F1305008M). Authors would like also to acknowledge the Nano'mat platform for providing the SEM equipment.

Received: January 16, 2017
Published online: March 6, 2017

[1] J. N. Coleman, M. Lotya, A. O'Neill, S. D. Bergin, P. J. King, U. Khan, K. Young, A. Gaucher, S. De, R. J. Smith, I. V. Shvets, S. K. Arora, G. Stanton, H.-Y. Kim, K. Lee, G. T. Kim, G. S. Duesberg, T. Hallam, J. J. Boland, J. J. Wang, J. F. Donegan, J. C. Grunlan, G. Moriarty, A. Shmeliov, R. J. Nicholls, J. M. Perkins, E. M. Grieveson, K. Theuwissen, D. W. McComb, P. D. Nellist, V. Nicolosi, *Science* **2011**, *331*, 568.
[2] Q. H. Wang, K. Kalantar-Zadeh, A. Kis, J. N. Coleman, M. S. Strano, *Nat. Nanotechnol.* **2012**, *7*, 699.
[3] M. Chhowalla, H. S. Shin, G. Eda, L.-J. Li, K. P. Loh, H. Zhang, *Nat. Chem.* **2013**, *5*, 263.
[4] D. Jariwala, V. K. Sangwan, L. J. Lauhon, T. J. Marks, M. C. Hersam, *ACS Nano* **2014**, *8*, 1102.
[5] A. Splendiani, L. Sun, Y. Zhang, T. Li, J. Kim, C.-Y. Chim, G. Galli, F. Wang, *Nano Lett.* **2010**, *10*, 1271.
[6] D. Xiao, G.-B. Liu, W. Feng, X. Xu, W. Yao, *Phys. Rev. Lett.* **2012**, *108*, 196802.
[7] M.-L. Tsai, S.-H. Su, J.-K. Chang, D.-S. Tsai, C.-H. Chen, C.-I. Wu, L.-J. Li, L.-J. Chen, J.-H. He, *ACS Nano* **2014**, *8*, 8317.
[8] M. Buscema, G. Steele, H. J. van der Zant, A. Castellanos-Gomez, *Nano Res.* **2014**, *7*, 561.
[9] C. Gong, C. Huang, J. Miller, L. Cheng, Y. Hao, D. Cobden, J. Kim, R. S. Ruoff, R. M. Wallace, K. Cho, X. Xu, Y. J. Chabal, *ACS Nano* **2013**, *7*, 11350.
[10] S. Bertolazzi, J. Brivio, A. Kis, *ACS Nano* **2011**, *5*, 9703.
[11] P. Johari, V. B. Shenoy, *ACS Nano* **2012**, *6*, 5449.
[12] K. He, C. Poole, K. F. Mak, J. Shan, *Nano Lett.* **2013**, *13*, 2931.
[13] B. Amin, T. P. Kaloni, U. Schwingenschlogl, *RSC Adv.* **2014**, *4*, 34561.
[14] W. S. Yun, S. W. Han, S. C. Hong, I. G. Kim, J. D. Lee, *Phys. Rev. B* **2012**, *85*, 033305.
[15] H. Peelaers, C. G. Van de Walle, *Phys. Rev. B* **2012**, *86*, 241401.
[16] Y. Wang, C. Cong, W. Yang, J. Shang, N. Peimyoo, Y. Chen, J. Kang, J. Wang, W. Huang, T. Yu, *Nano Res.* **2015**, *8*, 2562.
[17] J. Feng, X. Qian, C.-W. Huang, J. Li, *Nat. Photonics* **2012**, *6*, 866.
[18] D. Lloyd, X. Liu, J. W. Christopher, L. Cantley, A. Wadehra, B. L. Kim, B. B. Goldberg, A. K. Swan, J. S. Bunch, *Nano Lett.* **2016**, *16*, 5836.
[19] A. Castellanos-Gomez, R. Roldán, E. Cappelluti, M. Buscema, F. Guinea, H. S. J. van der Zant, G. A. Steele, *Nano Lett.* **2013**, *13*, 5361.
[20] H. Shi, R. Yan, S. Bertolazzi, J. Brivio, B. Gao, A. Kis, D. Jena, H. G. Xing, L. Huang, *ACS Nano* **2013**, *7*, 1072.
[21] A. Castellanos-Gomez, M. Poot, G. A. Steele, H. S. J. van der Zant, N. Agraït, G. Rubio-Bollinger, *Adv. Mater.* **2012**, *24*, 772.
[22] T. Jin, J. Kang, E. Su Kim, S. Lee, C. Lee, *J. Appl. Phys.* **2013**, *114*, 164509.
[23] S. Mouri, Y. Miyauchi, K. Matsuda, *Nano Lett.* **2013**, *13*, 5944.
[24] X. Zheng, Y. Zhang, R. Chen, X. a. Cheng, Z. Xu, T. Jiang, *Opt. Express* **2015**, *23*, 15616.
[25] M.-Y. Li, Y. Shi, C.-C. Cheng, L.-S. Lu, Y.-C. Lin, H.-L. Tang, M.-L. Tsai, C.-W. Chu, K.-H. Wei, J.-H. He, W.-H. Chang, K. Suenaga, L.-J. Li, *Science* **2015**, *349*, 524.
[26] P. Zu, Z. K. Tang, G. K. L. Wong, M. Kawasaki, A. Ohtomo, H. Koinuma, Y. Segawa, *Solid State Commun.* **1997**, *103*, 459.
[27] Q. Peng, S. De, *Phys. Chem. Chem. Phys.* **2013**, *15*, 19427.
[28] W.-C. Sun, Y.-C. Yeh, C.-T. Ko, J.-H. He, M.-J. Chen, *Nanoscale Res. Lett.* **2011**, *6*, 556.
[29] Z. Liu, M. Amani, S. Najmaei, Q. Xu, X. Zou, W. Zhou, T. Yu, C. Qiu, A. G. Birdwell, F. J. Crowne, R. Vajtai, B. I. Yakobson, Z. Xia, M. Dubey, P. M. Ajayan, J. Lou, *Nat. Commun.* **2014**, *5*, 5246.
[30] S. Mouri, Y. Miyauchi, K. Matsuda, *Nano Lett.* **2013**, *13*, 9544.
[31] N. Peimyoo, W. Yang, J. Shang, X. Shen, Y. Wang, T. Yu, *ACS Nano* **2014**, *8*, 11320.
[32] J. Choi, H. Zhang, J. H. Choi, *ACS Nano* **2016**, *10*, 1671.
[33] H. J. Conley, B. Wang, J. I. Ziegler, R. F. Haglund, S. T. Pantelides, K. I. Bolotin, *Nano Lett.* **2013**, *13*, 3626.
[34] S. B. Desai, G. Seol, J. S. Kang, H. Fang, C. Battaglia, R. Kapadia, J. W. Ager, J. Guo, A. Javey, *Nano Lett.* **2014**, *14*, 4592.
[35] X. Peng, Q. Wei, A. Copple, *Phys. Rev. B* **2014**, *90*, 085402.
[36] G. A. Rodrigo, Z. Xiaoliang, M. Saikat, P. Ravindra, R. R. Alexandre, P. K. Shashi, *J. Phys.: Condens. Matter* **2013**, *25*, 195801.
[37] Y.-C. Wu, C.-H. Liu, S.-Y. Chen, J.-Y. Shih, P.-H. Ho, C.-W. Chen, C.-T. Liang, W.-H. Wang, *Sci. Rep.* **2015**, *5*, 11472.
[38] J. Kang, S. Tongay, J. Zhou, J. Li, J. Wu, *Appl. Phys Lett.* **2013**, *102*, 012111.
[39] H.-L. Liu, H. Guo, T. Yang, Z. Zhang, Y. Kumamoto, C.-C. Shen, Y.-T. Hsu, L.-J. Li, R. Saito, S. Kawata, *Phys. Chem. Chem. Phys.* **2015**, *17*, 14561.
[40] J.-U. Lee, K. Kim, H. Cheong, *2D Mater.* **2015**, *2*, 044003.
[41] X. H. Wang, J. Q. Ning, C. C. Zheng, B. R. Zhu, L. Xie, H. S. Wu, S. J. Xu, *J. Mater. Chem. C* **2015**, *3*, 2589.